Theoretical studies on the quercetin interactions in the oil-in-water F127 microemulsion: A DFT and MD investigation

Journal of Molecular Liquids 383 (2023) 122037

Contents lists available at ScienceDirect

Journal of Molecular Liquids

journal homepage: www.elsevier.com/locate/molliq

Theoretical studies on the quercetin interactions in the oil-in-water F127 microemulsion: A DFT and MD investigation

Mahdiye Poorsargol [a,*], Abbas Rahdar [b], Francesco Baino [c,*], Pouya Karimi [d]

[a] Department of Chemistry, School of Basic Sciences, University of Zabol, Zabol, Iran
[b] Department of Physics, School of Basic Sciences, University of Zabol, Zabol, Iran
[c] Institute of Materials Physics and Engineering, Department of Applied Science and Technology, Politecnico di Torino, Torino, Italy
[d] Department of Chemistry, School of Basic Sciences, University of Zabol, Zabol, Iran

ARTICLE INFO

Keywords:
Microemulsion
Quercetin
Molecular dynamics
Drug release

ABSTRACT

Quercetin (Q) has attracted the attention of researchers for potential applications in advanced therapeutic treatments due to its antioxidant attributes and renal tissue improvement. F127-based oil-in-water microemulsions improved the bioavailability of Q and showed greater retention and more stable release. In this study, Q-loaded microemulsion was designed with the help of simulation techniques. The mechanism of action of Q was investigated in the bulk and microemulsion forms. The simulation results show the fast accumulation of Q molecules around 2,2-diphenyl-1-picrylhydrazyl (DPPH) molecules (free radicals) in bulk form and the slow accumulation of Q molecules around DPPH in microemulsion form. The stable release of Q in microemulsion form was found to be due to the powerful van der Waals (vdW) interactions between Q and F127. For a better and deeper understanding of the nature of mutual interactions between Q (enol and keto forms) and F127, quantum mechanical calculations were performed at the B3LYP/6-31G(d,p) level of theory. In particular, atoms in molecules (AIM) and natural bond orbital (NBO) analyses were performed to evaluate the strength of the interactions between Q and F127. The results showed that the formation of a strong hydrogen bond (HB) between Q_{enol} and F127 stabilizes the microemulsion system and can contribute to the better performance of Q microemulsion compared to free Q in bulk.

1. Introduction

Recently, flavonoids and their derivatives have attracted the attention of the biomedical community due to their favorable biological attributes (e.g., antioxidant, antimicrobial, anticancer, cardioprotective) [1,2]. Quercetin (Q) is one of the most common plant flavonoids found in various fruits, seeds, and vegetables, such as apples, grapes, legumes, pepper, cabbage, broccoli, and green tea [3–5]. Currently, Q is largely used as a food supplement and a phytochemical drug with antioxidant, anti-diabetic, anti-inflammatory and anti-proliferative effects [6]. The strong antioxidant activity of Q is due to its special structure which removes free radicals. Q is the most potent scavenger of reactive oxygen species and reduces oxidative stress in the renal tissue [7]. The antioxidant attributes of Q against oxidative stress caused by sodium fluoride were investigated in rats [8,9]. The antioxidant activity of Q showed a significant protective effect in the liver and kidneys of rats. Moreover, Q has also shown various benefits in the improvement of kidney fibrosis [10,11]. Nonetheless, due to the poor bioavailability of Q, the use of this powerful antioxidant remains a potential rather than an actual undertaking [12,13]. Therefore, providing new simple methods to improve its solubility is a challenge.

Nanotechnology is an emerging field which is developing rapidly and finding wide applications in biomedicine, including improved bioavailability and solubility of drugs, protection against physicochemical degradation, increased therapeutic activities, strengthening stability, and stable delivery of drugs [14–19]. Nanoscale materials have been found to exhibit attractive physical and chemical properties as well as biological potentials [20–23]. The size of these nanomaterials ranges from 10 to 1000 nm, indicating a significant reduction in the size of the active pharmaceutical ingredient (API) particles. Smaller API particles significantly increase the dissolution rate of the drug, consequently increasing its bioavailability to a large extent [24]. Thus, this technology can be very promising for increasing bioavailability and improving the solubility of poorly soluble drugs.

* Corresponding authors.
E-mail addresses: poorsargol.m@uoz.ac.ir (M. Poorsargol), a.rahdar@uoz.ac.ir (A. Rahdar), francesco.baino@polito.it (F. Baino), pkarimi@uoz.ac.ir (P. Karimi).

https://doi.org/10.1016/j.molliq.2023.122037
Received 28 January 2023; Received in revised form 3 May 2023; Accepted 4 May 2023
Available online 9 May 2023

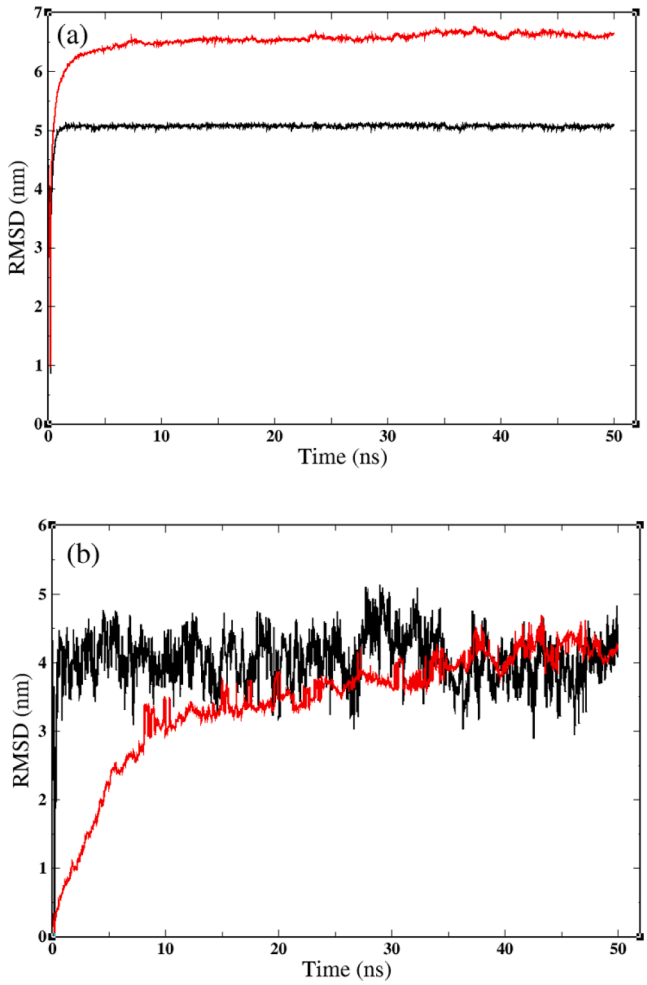

Fig. 1. RMSD plots of (a) total system for two simulated systems: bulk (black line) and microemulsion (red line) and (b) Q in two simulated systems: bulk (black line) and microemulsion (red line) as a function of the simulation time.

Microemulsions are potential drug delivery systems consisting of oil, surfactant (non-ionic or anionic), cosurfactants and water. They are biocompatible and biodegradable and can be easily produced by a low-cost process [25,26]. These versatile nano-formulations have the ability to encapsulate a large number of hydrophobic and hydrophilic drug molecules and prevent the enzymatic degradation of drugs, thus increasing their bioavailability [27]. Oil-in-water microemulsions can improve the oral bioavailability of these drugs by further dissolving hydrophobic drugs, ultimately leading to improved delivery of drug molecules to the target tissues [13,28]. Recently, our group used oil-in-water microemulsion based on Pluronic F127 surfactant to encapsulate Q and improve its bioavailability [29]. The antioxidant activity of free Q in bulk and Q microemulsion against 2,2-diphenyl-1-picrylhydrazyl (DPPH) free radicals was compared. The results showed that Q was released 16.34 times faster in bulk form than in microemulsion form. Also, the protective effects of oil-in-water Q-loaded microemulsion and free Q against renal damage caused by gentamicin (GM) and oxidative stress were investigated in rats. The results of the study revealed the beneficial effects of dietary nano-encapsulated Q (NEQ) for protecting rats from renal damage caused by GM. The antioxidant effect of NEQ was found to play a role in improving the renal functional biomarkers, histological structure, and reduce oxidative damage in GM-treated rats to a large extent.

Experimental studies provide very valuable results; however, investigating the intermolecular interactions at the microscopic level, which determine the behavior of such systems, is very difficult or impossible by experimental tests. In this regard, molecular dynamics (MD) simulation and quantum mechanical methods are very powerful techniques for gathering information at the microscopic level about the systems under investigation [30–36]. Therefore, these methods can be used to complement experimental tests and provide a clear picture of intermolecular interactions on a microscopic scale. Thus, following the aforementioned study, computational analyses were performed in the present work to gain a deep insight into the nature of the Q interactions inside nanocarrier, which can explain the higher retention and prolonged release of the Q molecules. In this research, the behavior of Q was investigated in bulk and microemulsion forms using MD simulation methods. Also, the intermolecular interactions in bulk and microemulsion forms were observed using MD simulation and quantum calculations. The present study provides detailed information on the nature of these interactions at the molecular level.

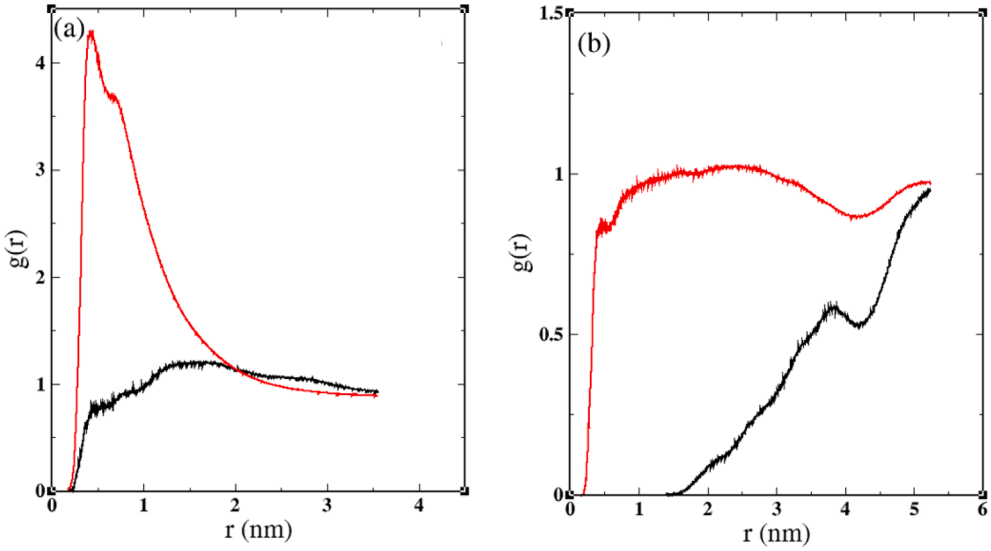

Fig. 2. Radial distribution function, g(r) of Q around DPPH for two simulated systems: (a) bulk and (b) microemulsion in two states before simulation equilibrium (black line) and after simulation equilibrium (red line).

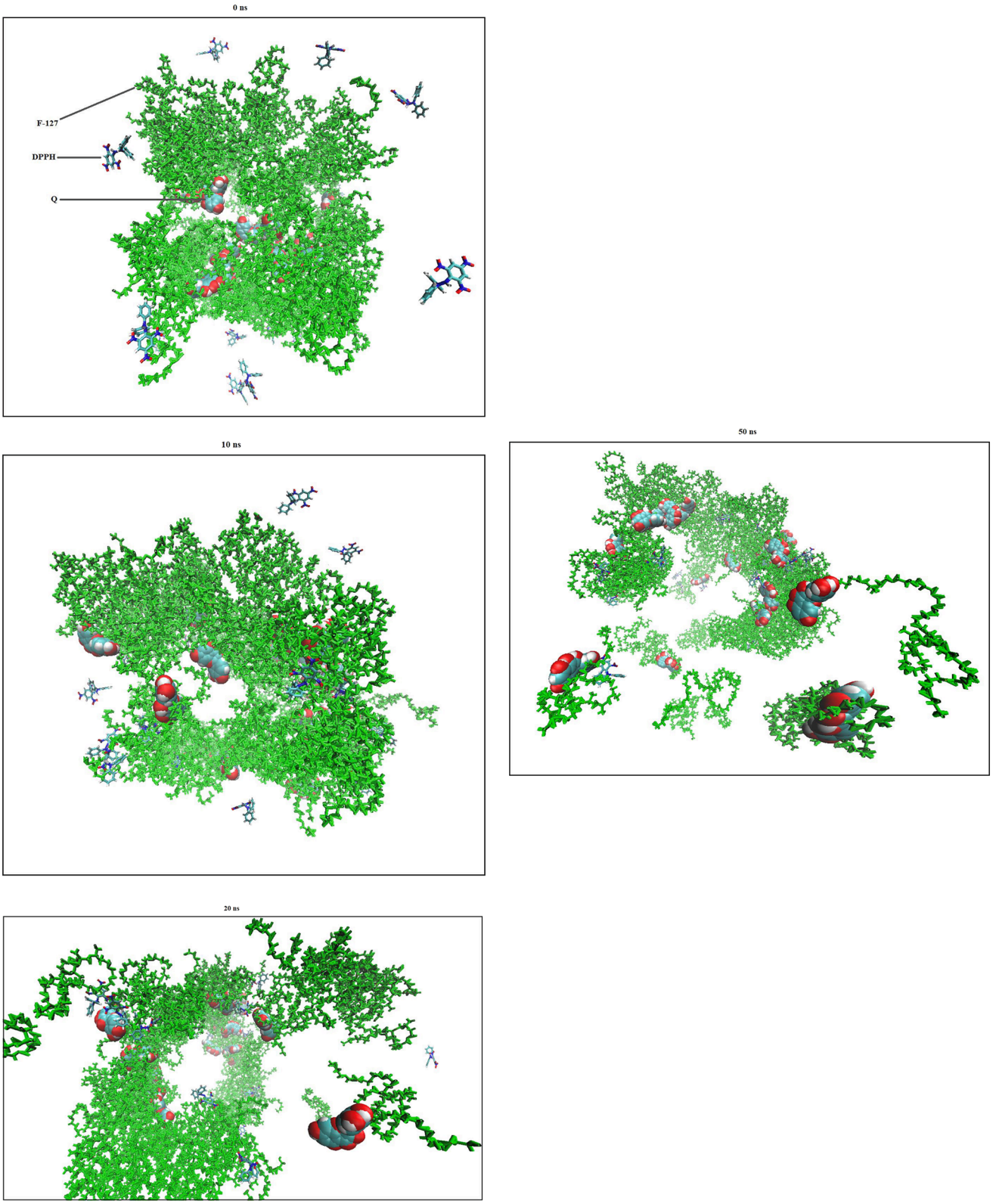

Fig. 3. Snapshot pictures during MD simulations of microemulsion system at t = 0 ns, 10 ns, 20 ns, and 50 ns. Methanol and ethyl-butyrate molecules have been removed for clarity.

2. Methods

2.1. Simulation methodology

MD simulation has been used to study the behavior of Q in bulk and microemulsion forms. MD is the representation of molecules and atoms using a number of classical degrees of freedom and interaction energies via potential energies called force fields. MD acts based on the integration of Newton second law of motion [37]. Computer simulation is a powerful tool for gathering microscopic information about the systems

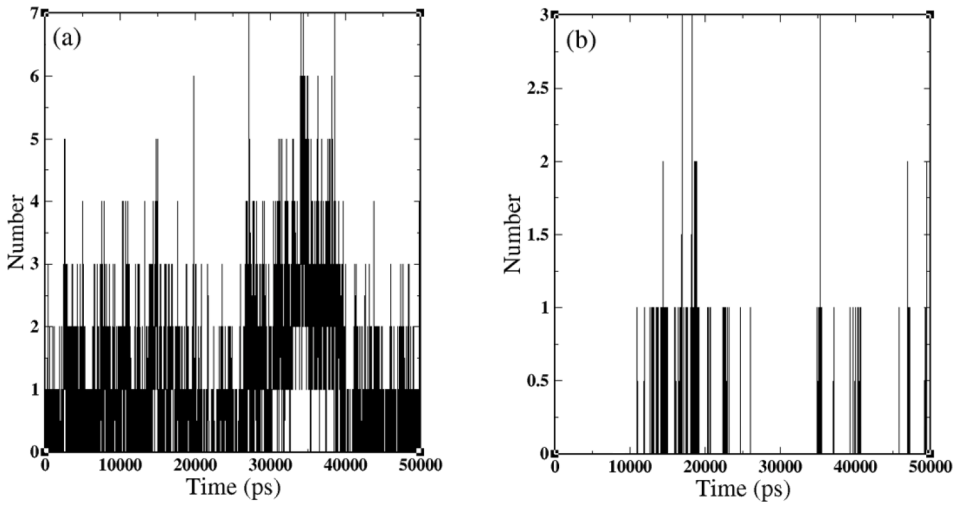

Fig. 4. Number of HBs between Q and DPPH for two simulated systems: (a) bulk and (b) microemulsion as a function of the simulation time.

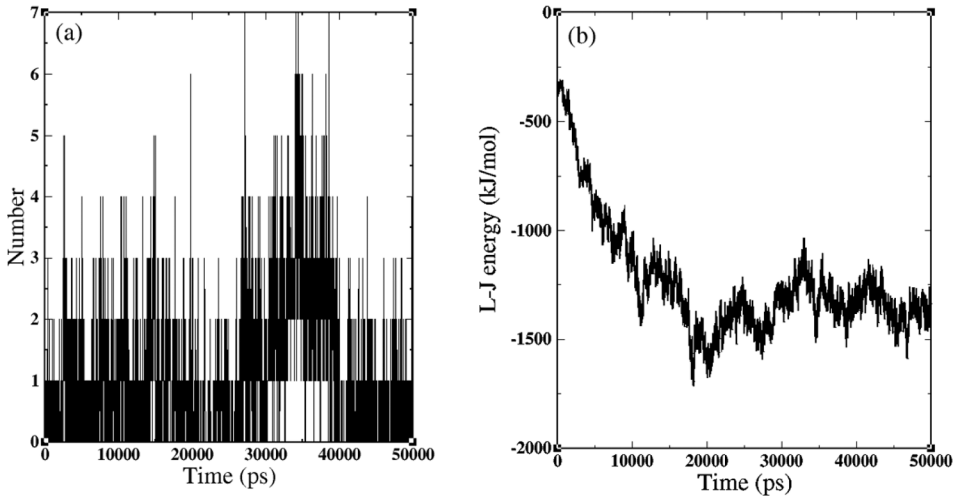

Fig. 5. (a) Number of HBs between Q and F127 in the microemulsion system as a function of the simulation time (b) The L-J energy between Q and F127 in term of simulation time.

Table 1
The average electrostatic and L-J energies between different groups, including Q, DPPH and F127 (kJ/mol).

System	electrostatic energy between Q and DPPH	L-J energy between Q and DPPH	electrostatic energy between Q and F127	L-J energy between Q and F127
bulk	−39.85	−316.11	–	–
micro	−2.78	−20.50	−372.05	−1237.50

under investigation. One of the systems investigated in this study contained 15 Q molecules and 15 DPPH molecules, which were randomly dispersed in a box containing methanol using Packmol [38]. The other studied system comprised a microemulsion in a box containing methanol and DPPH. The microemulsion comprised 15 Q molecules randomly dispersed in ethyl-butyrate and covered with the F127 surfactant.

The topology and coordinate files were created using ANTECHAMBER of AMBERTools [39] according to the general AMBER force field (GAFF) [40] and later on converted to GROMACS topology and coordinate files using an acpype script. Then, these parameters were added to the amber99sb force field. MD simulations were performed using GROMACS version 4.6 [41]. Before starting MD simulation, energy minimization was carried out using the steepest descent algorithm. Afterwards, the system went through NVT ensemble MD simulation at constant temperature of 298 K for 100 ps and then continued employing NPT ensemble for 100 ps at a constant temperature of 298 K and constant pressure of 1 bar by using Nose–Hoover thermostat and Parrinello–Rahman barostat [42,43]. MD simulation was performed by NPT for 50 ns and the used integration time step in the MD simulation was 1 fs. Equations of motion were integrated using the Verlet algorithm [44]. Long-range electrostatic interactions were calculated using the particle mesh Ewald (PME) method, and the cut-off distance for the van der Waals (vdW) interactions was taken as 1.2 nm [45]. Periodic boundary conditions were used in all three directions and the trajectories, velocities and forces on the constituent atoms of the system were stored at 10 ps intervals.

2.2. Quantum mechanics

The interactions between Q and F127 were examined by using Density Functional Theory (DFT) calculations. The molecular structures of Q (enol and keto forms) and a unit of the F127 surfactant polymer chain were designed in GaussView5.0. All geometries, including monomers and binary complexes of F-Q were optimized at the

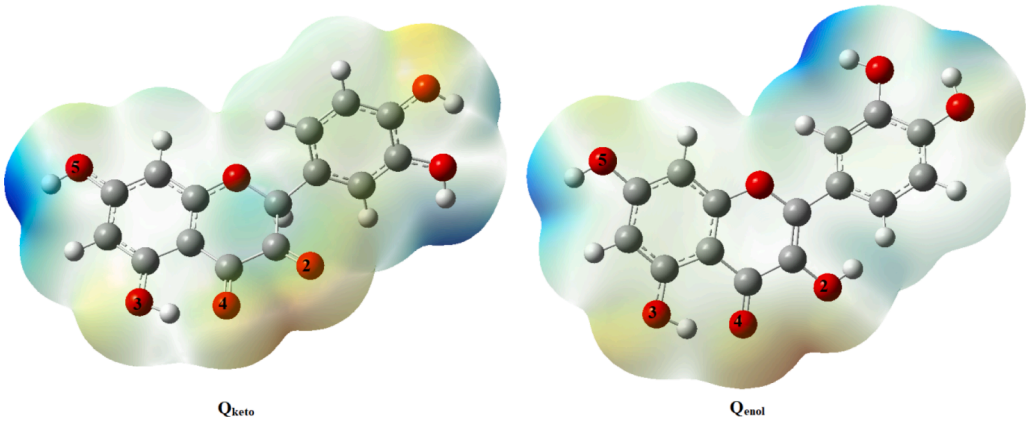

Fig. 6. MEP maps of Q drug.

theoretical level of B3LYP/6-31G(d,p) in the Gaussian09 program package [46]. The topological analysis of the electron charge density was performed at the B3LYP/6-31G(d,p) level of theory in AIM2000 using atoms in molecules (AIM) method [47]. The natural bond orbital (NBO) program in Gaussian09 was used to perform a population analysis of the optimized structures and obtained wave functions at the same level of theory [48]. The interaction energy (ΔE) of the F-Q binary complex is calculated using the difference between the energy of the binary complex and the sum of the energies of Q and F127 monomers. Binding energy (-ΔE) is a metric for evaluating the Q to F127 binding strength.

3. Results and discussion

3.1. MD simulation

First, the equilibrium of the simulated systems was considered. The root mean square deviation (RMSD) was analyzed to investigate the equilibrium of the systems during the structural changes. RMSD curves (bulk and microemulsion systems) were plotted for the total system as a function of simulation time (Fig. 1). Fig. 1a shows that RMSD curve of bulk system has flattened after 3 ns and RMSD curve of microemulsion system after 10 ns, indicating that the simulation systems have reached equilibrium. The RMSD curves of the Q was also graphed in two simulated systems to observe the Q stability throughout the simulation time (Fig. 1b). In the bulk system, the time to reach stability was shorter for Q according to its curve in Fig. 1b (5 ns), suggesting its faster flattening. Q stabilization can be explained by its interactions with DPPH. The deviations of the Q curve were greater in the microemulsion system, and the complexity of the micro-structure caused the stability to be achieved approximately after 20 ns. The higher displacement of Q molecules in this system also postponed the stability. In the bulk system, Q therefore appeared to interact with DPPH faster and easier.

To further investigate this subject, the distribution of Q molecules around DPPH was obtained as the radial distribution function, g(r); the diagrams before simulation equilibrium and after simulation equilibrium are displayed in Fig. 2. The g(r) can be analyzed to investigate interactions between particles, determine the structural properties of the simulated system and explain the possibility of interactions between a particle and its closest neighbors. The values of g(r) in Fig. 2a showed a significant increase in the density of Q molecules around DPPH as compared to the situation before simulation equilibrium in the bulk system, suggesting the rapid and easy accumulation of Q molecules around DPPH and interactions of these molecules with DPPH. The values of g(r) in Fig. 2b showed a negligible increase in the density of Q molecules around DPPH as compared to the situation before simulation equilibrium. The low accumulation of Q molecules around DPPH at the end of the simulation indicated a slow Q release in the microemulsion form. This simulation observation is in line with the experimental observations reported in [29], further confirming that Q is released much faster in bulk form than in microemulsion form. The release of Q in the microemulsion form during the MD simulation is displayed in Fig. 3. The snapshots taken from the simulation confirm the g(r) and RMSD curves of Q and indicate that Q molecules were released from the microemulsion 20 ns after the onset of the simulation. Based on the microemulsion structure, the slow release of Q in the microemulsion indicates the interaction of Q molecules with F127 molecules.

To further investigate the interactions between Q, DPPH and F127 molecules, analysis of the hydrogen bonds (HBs) formed between these molecules was performed along the simulation trajectory. A HB is considered strong in case the distance between the acceptor and hydrogen does not exceed 3.5 Å and the angle between the acceptor-hydrogen and hydrogen-donor vectors does not exceed 30°. Fig. 4 shows the number of HBs between Q and DPPH in the simulated systems versus the simulation time along the simulation trajectories. Fig. 4a shows rapid increases with the simulation time in the number of interactions and subsequent HBs formed between Q molecules and DPPH in the bulk system. This observation is consistent with the g(r) diagram in Fig. 2a, which shows a rapid increase in the density of Q molecules around DPPH. Fig. 4b shows that no HBs formed between Q molecules and DPPH in the first 10 ns of the simulation, which suggested the absence of Q in the neighborhood of DPPH, and that few HBs formed after 10 ns. In line with the data of the g(r) diagram in Fig. 2b, the small number of HBs in the microemulsion system demonstrated the decrease in the rate of Q release in the microemulsion form. Fig. 5a shows the number of HBs formed between Q molecules and F127 in the microemulsion system in terms of the simulation time, suggesting interactions between Q and F127. Table 1 presents the calculated average electrostatic and Lennard-Jones (L-J) energies between different groups, including Q, DPPH and F127, along the simulation trajectories for the bulk and microemulsion systems; for instance, the L-J energy between Q and F127 in the microemulsion system is shown in Fig. 5b as a function of the simulation time. According to Table 1, the L-J energy value between Q and DPPH in the bulk system (−316.11 kJ/mol) showed that vdW forces significantly contribute to interactions between Q and DPPH. A decrease in this energy to −20.50 kJ/mol in the microemulsion system therefore showed a significant reduction in vdW interactions between Q and DPPH. Moreover, the L-J energy value of −1237.50 kJ/mol between Q and F127 in the microemulsion system showed strong vdW interactions between Q and F127. Therefore, strong vdW interactions between Q and F127 may partly explain the slow release of Q in the microemulsion form.

3.2. Quantum mechanics calculations

The simulations indicated that Q has strong interactions with F127 in

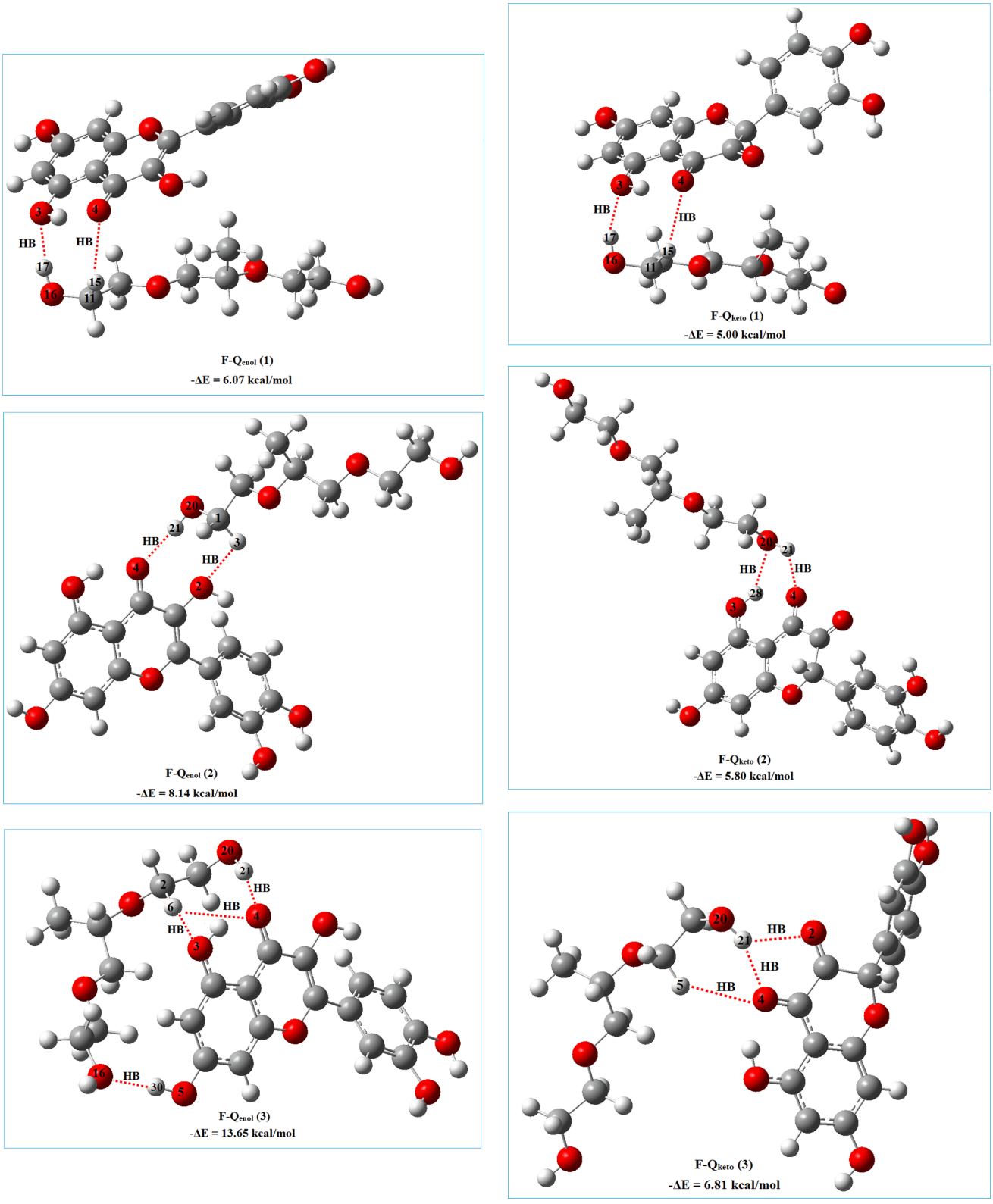

Fig. 7. The optimized structures of the studied complexes and the values of binding energy (in kcal/mol).

the microemulsion system. Thus, quantum mechanics calculations helped gain a better understanding of the nature of these interactions at the molecular level.

Given the possibility of enol-keto tautomerization of Q and since the interactions of these two forms affect stability [49], this section has examined the role of both forms of Q on the stability. The molecular electrostatic potential (MEP) maps of Q (enol and keto forms) were plotted, which show that the electron-rich positions are located on the O_2, O_3 and O_4 atoms of the Q drug (see Fig. 6). Because they are prone to interaction with the F127, we focused on these positions and examined all possible positions for the Q and F127 interaction. The optimized structures of the complexes, as well as the binding energy values are

Table 2
HB lengths (Å) and the topological properties of the complexes (au).

Complex	HB	Bond length	ρ_{BCP}	$\nabla^2\rho_{BCP}$	G_{BCP}	V_{BCP}	H_{BCP}
F-Q_{enol} (1)	O_{16}-H_{17}…O_3	2.024	0.02212	−0.01490	0.01599	−0.01708	−0.00108
	C_{11}-H_{15}…O_4	2.734	0.00573	−0.00502	0.004214	−0.00340	0.00081
F-Q_{enol} (2)	O_{20}-H_{21}…O_4	1.951	0.02476	−0.01763	0.01821	−0.01880	−0.00059
	C_1-H_3…O_2	2.877	0.00478	−0.00468	0.00382	−0.00296	0.00086
F-Q_{enol} (3)	O_{20}-H_{21}…O_4	1.959	0.02373	−0.01716	0.01764	−0.01812	−0.00048
	O_5-H_{30}…O_{16}	1.842	0.03216	−0.02250	0.02306	−0.02362	−0.00056
	C_2-H_6…O_3	2.773	0.00549	−0.00457	0.00382	−0.00306	0.00076
	C_2-H_6…O_4	2.912	0.00443	−0.00421	0.00334	−0.00249	0.00085
	C_{10}-H_{12}…C_{18}	2.736	0.00775	−0.00575	0.00471	−0.00367	0.00104
F-Q_{keto} (1)	O_{16}-H_{17}…O_3	2.035	0.021421	−0.014804	0.015734	−0.01666	−0.00093
	C_{11}-H_{15}…O_4	2.961	0.003538	−0.003284	0.002562	−0.00184	0.00072
F-Q_{keto} (2)	O_{20}-H_{21}…O_4	2.057	0.019569	−0.018590	0.017652	−0.01671	0.00094
	O_3-H_{28}…O_{20}	2.165	0.016944	−0.0123552	0.012880	−0.01340	−0.00052
F-Q_{keto} (3)	O_{20}-H_{21}…O_4	2.087	0.018887	−0.013333	0.013951	−0.01456	−0.00061
	O_{20}-H_{21}…O_2	2.543	0.007425	−0.007548	0.006413	−0.00527	0.00114
	C_2-H_5…O_4	2.788	0.004903	−0.004586	0.003770	−0.00295	0.00082

presented in Fig. 7. The binding energies of the F-Q_{enol} (1), F-Q_{enol} (2), and F-Q_{enol} (3) complexes are 6.07, 8.14, and 13.65 kcal/mol, respectively. Evidently, the most stable complex is F-Q_{enol} (3) with the highest binding energy. Depending on the orientation of F127 and Q_{enol} relative to each other after optimization, (O_{16}-H_{17}…O_3) and (C_{11}-H_{15}…O_4) hydrogen bonding (HB) interactions exist in the F-Q_{enol} (1) complex, which create a seven-membered ring in this complex. There are (O_{20}-H_{21}…O_4) and (C_1-H_3…O_2) interactions in the F-Q_{enol} (2) complex, which create an eight-membered ring in it. The (O_{20}-H_{21}…O_4), (O_5-H_{30}…O_{16}), (C_2-H_6…O_3), (C_2-H_6…O_4), and (C_{10}-H_{12}…C_{18}) interactions also exist in the F-Q_{enol} (3) complex, which form two six-membered rings in it. Examination of the optimized structure of the F-Q_{enol} (3) complex shows that F127 around Q_{enol} is completely bent such that it can form a HB interaction with Q_{enol} through its O_{16} (see Fig. 7). It can thus be concluded that the formation of more HBs, as well as interaction between O_{16} of F127 and Q_{enol}, contributes to the greater stability of the F-Q_{enol} (3) complex. The binding energies of the F-Q_{keto} (1), F-Q_{keto} (2), and F-Q_{keto} (3) complexes are 5.00, 5.80, and 6.81 kcal/mol, respectively. Evidently, the binding energy values of the F-Q_{keto} complexes are lower than those of F-Q_{enol} complexes. As such, the keto form of Q has led to less stability of the desired complexes. The results show that there are (O_{16}-H_{17}…O_3) and (C_{11}-H_{15}…O_4) interactions in the F-Q_{keto} (1) complex, and similar to the F-Q_{enol} (1) complex, the O_3 and O_4 atoms of Q_{keto} are involved in forming an HB with F127. There are (O_{20}-H_{21}…O_4) and (O_3-H_{28}…O_{20}) interactions in the F-Q_{keto} (2) complex, in whose formation the O_4 atom of Q_{keto} and O_{20} atom of F127 are involved. There are (O_{20}-H_{21}…O_4), (O_{20}-H_{21}…O_2), and (C_2-H_5…O_4) interactions in the F-Q_{keto} (3) complex that the O_2 and O_4 atoms of Q_{keto} are involved in forming these bonds. On the other hand, there are two strong interactions in the F-Q_{enol} (3) complex, in which the O_4 atom of Q_{enol} and O_{16} atom of F127 participate. Therefore, it can be argued that the interaction between O_{16} of F127 and Q_{enol} leads to higher stability of the F-Q_{enol} (3) complex in comparison to other complexes. The H…O bond length for the mentioned HB interactions is given in Table 2. The H_{30}…O_{16} bond length in the F-Q_{enol} (3) complex is shorter than the length of all other HBs. This is in agreement with the above observation, which suggested that the (O_5-H_{30}…O_{16}) interaction is the strongest and has led to the stability of the F-Q_{enol} (3) complex. Therefore, with increasing the HB strength in the mentioned complexes, the H…O bond length declines.

The quantum theory of atoms in molecules (QTAIM) was adopted to interpret the topological properties of electron densities [50]. The AIM theory is a suitable method in quantum mechanics to examine various interactions. Topological parameters are used to detect the presence and describe the strength of HB interactions. Table 2 shows the values of electron density (ρ), the Laplacian of the electron density ($\nabla^2\rho$), electron kinetic energy density (G), electron potential energy density (V), and total electron energy density (H) at bond-critical points (BCPs) of all complexes calculated at the theoretical level of B3LYP/6-31G(d,p). The maximum electron density belongs to the BCP of H_{30}…O_{16} in the F-Q_{enol} (3) complex, which indicates that this HB is stronger. Both $\nabla^2\rho_{BCP}$ and H_{BCP} values are negative for (O_{16}-H_{17}…O_3), (O_{20}-H_{21}…O_4), (O_3-H_{28}…O_{20}), and (O_5-H_{30}…O_{16}) interactions, indicating that these HB interactions are strong while other HB interactions are weak. Fig. 8 shows the molecular graphs of the most stable complexes (F-Q_{enol}) namely BCPs (red spheres), ring-critical points (RCPs) (yellow spheres), and bond paths (pink lines). The aforementioned strong HB interactions are also demonstrated in the graphs.

Formation of HB and new rings in binary complexes leads to the transfer of the electron charge between Q and F127. Therefore, to better understand the source of stability in these complexes, we performed atomic charge analysis on binary complexes and monomers of Q and F127. Table 3 shows the charge (q) of the atoms participating in strong HB interactions. In the two complexes F-Q_{enol} (1) and F-Q_{enol} (2), the electron charge is transferred from Q_{enol} to F127. On the other hand, in the strong interaction (O_5-H_{30}…O_{16}) in the F-Q_{enol} (3) complex, the charge is transferred from F127 to Q_{enol}. This result indicates that the formation of six-membered ring affects the direction of charge transfer in F-Q_{enol} (3) complex. In the complexes F-Q_{keto}, the electron charge is transferred from Q_{keto} to F127. Table 3 shows that the charge of O atoms in all of the complexes is more negative than the charge of O atoms in the monomers. In addition, the charge of H atoms has become more positive with the formation of complexes. Evidently, the increase in the negative charge of the O atoms of the complexes is associated with an enhancement in the stability of the complexes. Furthermore, the increase in the positive charge of the H atoms of the complexes is accompanied by a rise in the stability of the complexes. The sum of the mentioned charges in the F-Q_{enol} and F-Q_{keto} binary complexes ($\sum q_{OHO}$) is presented in the Table 3. There is linear relationship between the binding energy values of the mentioned complexes and $\sum q_{OHO}$. Clearly, a decrease in the absolute value of $\sum q_{OHO}$ is associated with an increase in the binding energy values of the.

F-Q_{enol} and F-Q_{keto} complexes. Therefore, the charges of the atoms participating in HB interactions affect the stability of the F-Q_{enol} complexes. As can be discerned, in the most stable complex, i.e., F-Q_{enol} (3), the charge has been transferred to the O_5-H_{30} of Q_{enol} through the O_{16} atom of F127.

A population analysis was performed using the NBO method, which helps us gain a better insight into electron charge transfer between molecular orbitals in these binary complexes. Thus, the $E^{(2)}$ acceptor–donor stabilization energies for Lp(O) → σ^*_{OH} strong interactions of all complexes are calculated at the theoretical level of B3LYP/6-31G(d,p) (Table 4). It is worth highlighting that the interaction of Lp(O) to σ^*_{OH} in the two complexes F-Q_{enol} (1) and.

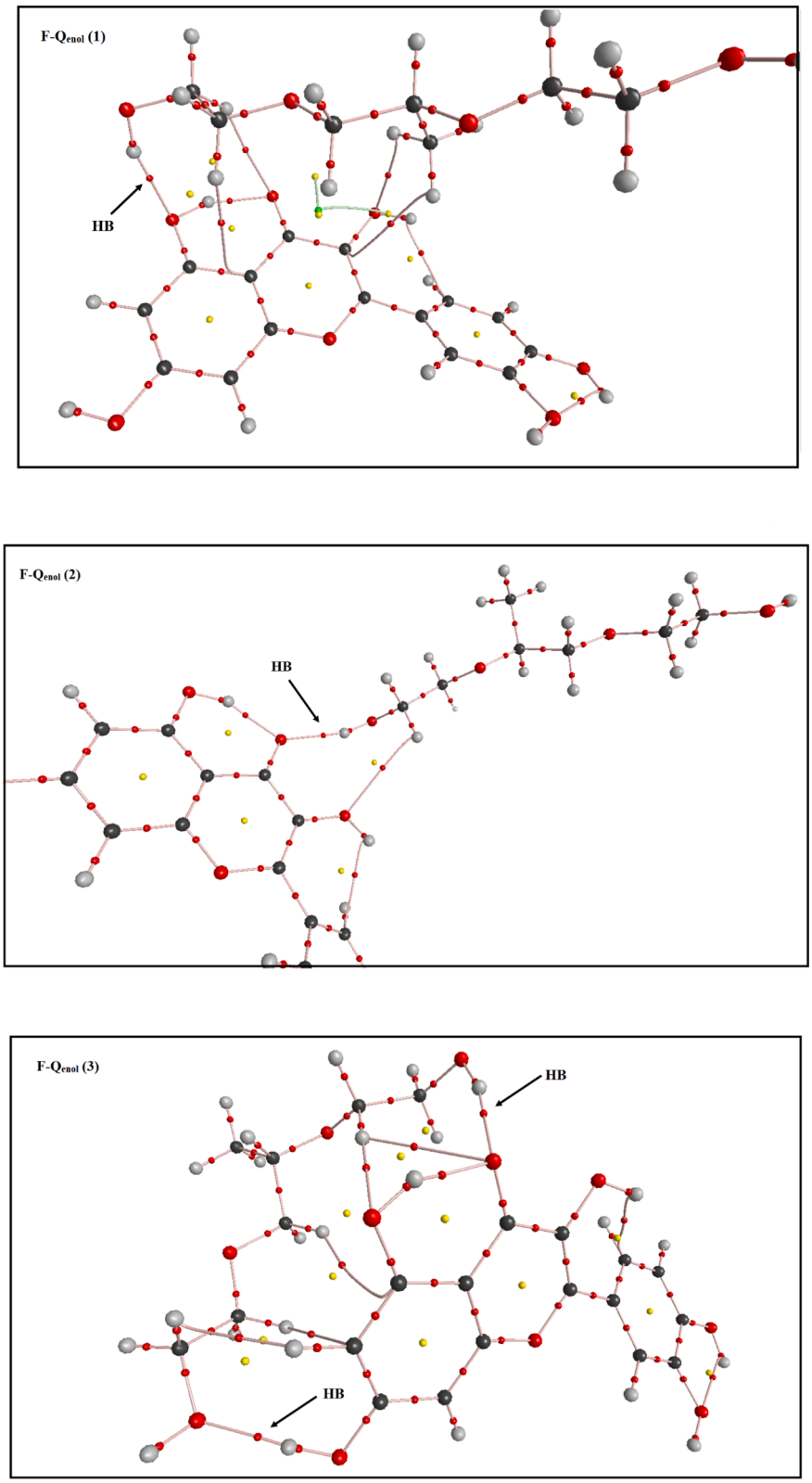

Fig. 8. The molecular graphs of the F-Q_{enol} complexes. The red and yellow spheres are BCPs and RCPs, respectively.

F-Q_{enol} (2) occurs only from Q_{enol} to F127, while this interaction occurs in the F-Q_{enol} (3) complex in both modes (from Q_{enol} to F127 and from F127 to Q_{enol}). Also, the interaction of Lp(O) to σ^*_{OH} in the complexes F-Q_{keto} (1), F-Q_{keto} (2), and F-Q_{keto} (3) occurs only from Q_{keto} to F127. The value of $E^{(2)}$ for this electron charge transfer in F-Q_{enol} (1) and F-Q_{enol} (2) complexes is 8.30 and 10.42 kcal/mol, respectively. In the F-Q_{enol} (3) complex, there are two strong interactions, such that the sum of $E^{(2)}$ values is equal to 25.21 kcal/mol. The $E^{(2)}$ values for the mentioned electron charge transfers in the F-Q_{keto} complexes are lower than corresponding values in the F-Q_{enol} complexes. A comparison of $E^{(2)}$ values for all the complexes shows that the highest $E^{(2)}$ value belongs to the F-Q_{enol} (3) complex with the greatest binding energy; thus, the electron

Table 3
The charge of atoms involving in HB interaction (in e).

	$q_{O\ (acceptor)}$	q_H	$q_{O\ (donor)}$	$\sum q_{OHO}$
F127	–	**	*	
Q_{enol}	***	**	–	
Q_{keto}	****	–	–	
F-Q_{enol} (1) (O_{16}-H_{17}…O_3)	−0.718	0.491	−0.775	−1.002
F-Q_{enol} (2) (O_{20}-H_{21}…O_4)	−0.648	0.508	−0.787	−0.927
F-Q_{enol} (3) (O_{20}-H_{21}…O_4)	−0.659	0.500	−0.775	−0.934
F-Q_{enol} (3) (O_5-H_{30}…O_{16})	−0.786	0.518	−0.700	−0.968
F-Q_{keto} (1) (O_{16}-H_{17}…O_3)	−0.708	0.489	−0.770	−0.989
F-Q_{keto} (2) (O_{20}-H_{21}…O_4)	−0.599	0.510	−0.781	−0.870
F-Q_{keto} (3) (O_{20}-H_{21}…O_4)	−0.608	0.496	−0.776	−0.888

* Charge of atoms O_{16} and O_{20} in F127 is −0.761 and −0.762 e, respectively.
** Charge of atoms H_{17}, H_{21} and H_{30} in F127 and Q_{enol} is 0.482, 0.482 and 0.497 e, respectively.
*** Charge of atoms O_3, O_4 and O_5 in Q_{enol} is −0.690, −0.615 and −0.681 e, respectively.
**** Charge of atoms O_3 and O_4 in Q_{keto} is −0.678 and −0.572 e, respectively.

Table 4
The charge transfer energies of complexes at B3LYP/6-31G(d,p) level (kcal/mol).

Complex	Charge transfer	$E^{(2)}$ (kcal/mol)
F-Q_{enol} (1)	$Lp(O_3) \rightarrow \sigma^*O_{16}H_{17}$	8.30
F-Q_{enol} (2)	$Lp(O_4) \rightarrow \sigma^*O_{20}H_{21}$	10.42
F-Q_{enol} (3)	$Lp(O_4) \rightarrow \sigma^*O_{20}H_{21}$	6.91
F-Q_{enol} (3)	$Lp(O_{16}) \rightarrow \sigma^*O_5H_{30}$	18.30
F-Q_{keto} (1)	$Lp(O_3) \rightarrow \sigma^*O_{16}H_{17}$	7.78
F-Q_{keto} (2)	$Lp(O_4) \rightarrow \sigma^*O_{20}H_{21}$	4.57
F-Q_{keto} (3)	$Lp(O_4) \rightarrow \sigma^*O_{20}H_{21}$	6.46

charge transfer from F127 surfactant to Q_{enol} play a key role in the stability of F-Q_{enol} (3) complex.

4. Conclusion

In this study, the MD simulation technique was used to investigate the behavior of Q in both bulk and microemulsion forms. The obtained results were quantified using representative simulation snapshots, RMSD plots, g(r) curves, HB analysis, and L-J and electrostatic energies. The simulation results showed that, in microemulsion form, Q molecules are released from within the nanomicelle over a longer period of time and accumulate around the DPPH molecules. The L-J energy analysis between Q and F127 in the microemulsion system indicates powerful vdW interactions between Q and F127. Quantum mechanical calculations were performed for a more accurate and detailed study of the interactions between Q (enol and keto forms) and F127. The AIM and NBO analyses were also performed on the systems under study. It was observed that the F-Q_{enol} complexes are more stable than the F-Q_{keto} complexes. The computational results revealed the formation of strong HBs between Q_{enol} and F127, during which the electron charge was transferred from F127 to Q_{enol} or vice versa. The electron charge transfer, from the Lp (O_{16}) orbital of F127 surfactant to the $\sigma^*O_5H_{30}$ orbital of Q_{enol}, influences on the stability of the F-Q_{enol} complex.

CRediT authorship contribution statement

Mahdiye Poorsargol: Conceptualization, Investigation, Writing – original draft. **Abbas Rahdar:** Conceptualization, Investigation, Writing – original draft, Supervision. **Francesco Baino:** Investigation, Writing – review & editing. **Pouya Karimi:** Investigation, Writing – review & editing.

Declaration of Competing Interest

The authors declare that they have no known competing financial interests or personal relationships that could have appeared to influence the work reported in this paper.

Data availability

Data will be made available on request.

References

[1] M. İkizler, N. Erkasap, S. Dernek, T. Kural, Z. Kaygisiz, Dietary polyphenol quercetin protects rat hearts during reperfusion: enhanced antioxidant capacity with chronic treatment, Anadolu Kardiyol. Derg. 7 (2007) 404–410.
[2] M.G.L. Hertog, P.C.H. Hollman, M.B. Katan, D. Kromhout, Intake of potentially anticarcinogenic flavonoids and their determinants in adults in The Netherlands, (1993).
[3] G. D'Andrea, Quercetin: a flavonol with multifaceted therapeutic applications? Fitoterapia 106 (2015) 256–271.
[4] J.V. Formica, W. Regelson, Review of the biology of quercetin and related bioflavonoids, Food Chem. Toxicol. 33 (1995) 1061–1080.
[5] G.R. Beecher, B.A. Warden, H. Merken, Analysis of tea polyphenols, Proc. Soc. Exp. Biol. Med. 220 (1999) 267–270.
[6] G.-E.-S. Batiha, A.M. Beshbishy, M. Ikram, Z.S. Mulla, M.E.A. El-Hack, A.E. Taha, A. M. Algammal, Y.H.A. Elewa, The pharmacological activity, biochemical properties, and pharmacokinetics of the major natural polyphenolic flavonoid: Quercetin, Foods. 9 (2020) 374.
[7] N. Oršolić, G. Gajski, V. Garaj-Vrhovac, D. Đikić, Z.Š. Prskalo, D. Sirovina, DNA-protective effects of quercetin or naringenin in alloxan-induced diabetic mice, Eur. J. Pharmacol. 656 (2011) 110–118.
[8] S.M. Nabavi, S.F. Nabavi, S. Eslami, A.H. Moghaddam, In vivo protective effects of quercetin against sodium fluoride-induced oxidative stress in the hepatic tissue, Food Chem. 132 (2012) 931–935.
[9] S.M. Nabavi, S.F. Nabavi, S. Habtemariam, A.H. Moghaddam, A.M. Latifi, Ameliorative effects of quercetin on sodium fluoride-induced oxidative stress in rat's kidney, Ren. Fail. 34 (2012) 901–906.
[10] J. Ren, J. Li, X. Liu, Y. Feng, Y. Gui, J. Yang, W. He, C. Dai, Quercetin inhibits fibroblast activation and kidney fibrosis involving the suppression of mammalian target of rapamycin and β-catenin signaling, Sci. Rep. 6 (2016) 1–11.
[11] H. Lu, L. Wu, L. Liu, Q. Ruan, X. Zhang, W. Hong, S. Wu, G. Jin, Y. Bai, Quercetin ameliorates kidney injury and fibrosis by modulating M1/M2 macrophage polarization, Biochem. Pharmacol. 154 (2018) 203–212.
[12] R. Conte, A. Calarco, A. Napoletano, A. Valentino, S. Margarucci, F. Di Cristo, A. Di Salle, G. Peluso, Polyphenols nanoencapsulation for therapeutic applications, J. Biomol. Res. Ther. 5 (2016).
[13] B. Salehi, L. Machin, L. Monzote, J. Sharifi-Rad, S.M. Ezzat, M.A. Salem, R. M. Merghany, N.M. El Mahdy, C.S. Kılıç, O. Sytar, Therapeutic potential of quercetin: new insights and perspectives for human health, ACS Omega 5 (2020) 11849–11872.
[14] A. Rahdar, M.R. Hajinezhad, S. Sargazi, M. Bilal, M. Barani, P. Karimi, G.Z. Kyzas, Biochemical effects of deferasirox and deferasirox-loaded nanomicellesin iron-intoxicated rats, Life Sci. 270 (2021), 119146.
[15] S.S. Das, P. Bharadwaj, M. Bilal, M. Barani, A. Rahdar, P. Taboada, S. Bungau, G. Z. Kyzas, Stimuli-responsive polymeric nanocarriers for drug delivery, imaging, and theragnosis, Polymers (Basel). 12 (2020) 1397.
[16] J.K. Sahni, S. Baboota, J. Ali, Promising role of nanopharmaceuticals in drug delivery, Pharma, Times 43 (2011) 16–18.
[17] M. Barani, M. Mirzaei, M. Torkzadeh-Mahani, A. Lohrasbi-Nejad, M. H. Nematollahi, A new formulation of hydrophobin-coated niosome as a drug carrier to cancer cells, Mater. Sci. Eng. C 113 (2020), 110975.
[18] M. Barani, M. Mirzaei, M. Torkzadeh-Mahani, M.H. Nematollahi, Lawsone-loaded Niosome and its antitumor activity in MCF-7 breast Cancer cell line: a Nano-herbal treatment for Cancer, DARU J. Pharm. Sci. 26 (2018) 11–17.
[19] M.R. Hajizadeh, H. Maleki, M. Barani, M.A. Fahmidehkar, M. Mahmoodi, M. Torkzadeh-Mahani, In vitro cytotoxicity assay of D-limonene niosomes: an efficient nano-carrier for enhancing solubility of plant-extracted agents, Res. Pharm. Sci. 14 (2019) 448.
[20] P. Carneiro, Simone Morais, P. Maria Carmo, Nanomaterials towards biosensing of Alzheimer's disease biomarkers, Nanomaterials 9 (12) (2019) 1663.
[21] Q. Wang, Guoqing Sui, X. Wu, T. Dengke, L. Zhu, S. Guan, H. Ran, Z. Wang, W. Hui, A sequential targeting nanoplatform for anaplastic thyroid carcinoma theranostics, Acta Biomater. 102 (2020) 367–383.
[22] T.M. Sim, D. Tarini, S.T. Dheen, B.H. Bay, D.K. Srinivasan, Nanoparticle-based technology approaches to the management of neurological disorders, Int. J. Mol. Sci. 21 (17) (2020) 6070.
[23] X. Wu, H. Yang, W. Yang, X. Chen, J. Gao, X. Gong, H. Wang, Y. Duan, D. Wei, J. Chang, Nanoparticle-based diagnostic and therapeutic systems for brain tumors, J. Mater. Chem. B 7 (31) (2019) 4734–4750.
[24] M. Sun, X. Su, B. Ding, X. He, X. Liu, A. Yu, H. Lou, G. Zhai, Advances in nanotechnology-based delivery systems for curcumin, Nanomedicine 7 (2012) 1085–1100.

[25] M.A. Aboudzadeh, E. Mehravar, M. Fernandez, L. Lezama, R. Tomovska, Low-energy encapsulation of α-tocopherol using fully food grade oil-in-water microemulsions, ACS Omega 3 (2018) 10999–11008.
[26] C.D. Candido, M.L. Campos, J.U.C.V. Assumpção, K.C. Pestana, E.C. Padilha, I. Z. Carlos, R.G. Peccinini, Biocompatible microemulsion modifies the tissue distribution of doxorubicin, J. Pharm. Sci. 103 (2014) 3297–3301.
[27] T.K. Giri, N.G. Goswami, V.K. Jha, Prospective and challenges of micro-emulsion as a novel carrier for drug delivery, J. PharmaSciTech. 2 (2013) 56–61.
[28] F.T.M.C. Vicentini, T.R.M. Simi, J.O. Del Ciampo, N.O. Wolga, D.L. Pitol, M. M. Iyomasa, M.V.L.B. Bentley, M.J.V. Fonseca, Quercetin in w/o microemulsion: in vitro and in vivo skin penetration and efficacy against UVB-induced skin damages evaluated in vivo, Eur. J. Pharm. Biopharm. 69 (2008) 948–957.
[29] A. Rahdar, P. Hasanein, M. Bilal, H. Beyzaei, G.Z. Kyzas, Quercetin-loaded F127 nanomicelles: Antioxidant activity and protection against renal injury induced by gentamicin in rats, Life Sci. 276 (2021), 119420.
[30] S. Sargazi, M.R. Hajinezhad, M. Barani, M. Mukhtar, A. Rahdar, F. Baino, P. Karimi, S. Pandey, F127/cisplatin microemulsions: In vitro, in vivo and computational studies, Appl. Sci. 11 (2021) 3006.
[31] M. Poorsargol, M. Alimohammadian, B. Sohrabi, M. Dehestani, Dispersion of graphene using surfactant mixtures: Experimental and molecular dynamics simulation studies, Appl. Surf. Sci. 464 (2019) 440–450, https://doi.org/10.1016/j.apsusc.2018.09.042.
[32] S. Shahraki, H.S. Delarami, M. Poorsargol, Z.S. Nezami, Structural and functional changes of catalase through interaction with Erlotinib hydrochloride. Use of Chou's 5-steps rule to study mechanisms, Spectrochim. Acta A Mol. Biomol. Spectrosc. 260 (2021), 119940.
[33] Z. Setayesh-Mehr, M. Poorsargol, HL-7 and HL-10 Peptides Stimulate Insulin Secretion in the INS-1 Insulinoma Cell Line through Incretin-Dependent Pathway and Increasing the Glucose Uptake in L6 Myoblast, Int. J. Pept. Res. Ther. 27 (2021) 2231–2244.
[34] A. Rahdar, M.R. Hajinezhad, M. Barani, S. Sargazi, M. Zaboli, E. Ghazy, F. Baino, M. Cucchiarini, M. Bilal, S. Pandey, Pluronic F127/Doxorubicin microemulsions: Preparation, characterization, and toxicity evaluations, J. Mol. Liq. 345 (2022), 117028.
[35] S. Roosta, S.J. Nikkhah, M. Sabzali, S.M. Hashemianzadeh, Molecular dynamics simulation study of boron-nitride nanotubes as a drug carrier: From encapsulation to releasing, RSC Adv. 6 (2016) 9344–9351, https://doi.org/10.1039/c5ra22945f.
[36] H. Roohi, A. Facehi, K. Ghauri, Adsorption of cytarabine and gemcitabine anticancer drugs on the BNNT surface: DFT and GD3-DFT approaches, Adsorption 26 (2020) 1365–1384.
[37] W.F. van Gunsteren, J. Dolenc, A.E. Mark, Molecular simulation as an aid to experimentalists, Curr. Opin. Struct. Biol. 18 (2008) 149–153.
[38] L. Martínez, R. Andrade, E.G. Birgin, J.M. Martínez, PACKMOL: A package for building initial configurations for molecular dynamics simulations, J. Comput. Chem. 30 (2009) 2157–2164.
[39] D.A. Case, T.A. Darden, T.E. Cheatham III, C.L. Simmerling, J. Wang, R.E. Duke, R. Luo, K.M. Merz, D.A. Pearlman, M. Crowley, AMBER 9, Univ. California, San Fr. 45 (2006).
[40] J. Wang, R.M. Wolf, J.W. Caldwell, P.A. Kollman, D.A. Case, Development and testing of a general amber force field, J. Comput. Chem. 25 (2004) 1157–1174.
[41] B. Hess, C. Kutzner, D. Van Der Spoel, E. Lindahl, GROMACS 4: algorithms for highly efficient, load-balanced, and scalable molecular simulation, J. Chem. Theory Comput. 4 (2008) 435–447.
[42] M. Parrinello, A. Rahman, Polymorphic transitions in single crystals: A new molecular dynamics method, J. Appl. Phys. 52 (1981) 7182–7190.
[43] S. Nosé, A molecular dynamics method for simulations in the canonical ensemble A molecular dynamics method for simulations in the canonical ensemblet, An Int. J. Interface Between Chem. Phys, Mol. Phys. 52 (1984) 255–268.
[44] L. Verlet, Computer" experiments" on classical fluids. I. Thermodynamical properties of Lennard-Jones molecules, Phys. Rev. 159 (1967) 98.
[45] T. Darden, D. York, L. Pedersen, Particle mesh Ewald: An N·log(N) method for Ewald sums in large systems, J. Chem. Phys. 98 (1993) 10089–10092, https://doi.org/10.1063/1.464397.
[46] M.J. Frisch, G.W. Trucks, H.B. Schlegel, G.E. Scuseria, M.A. Robb, J.R. Cheeseman, G. Scalmani, V. Barone, B. Mennucci, G.A. Petersson, Gaussian 09 citation, Gaussian Inc., Wallingford, 2013.
[47] R.F.W. Bader, Atoms in molecules, Acc. Chem. Res. 18 (1985) 9–15.
[48] E.D. Glendening, A.E. Reed, J.E. Carpenter, F. Weinhold, NBO, version 3.1, Gaussian, Inc. Pittsburgh, PA. (2003).
[49] A. Fusina, P. Degot, D. Touraud, W. Kunz, V. Nardello-Rataj, Enhancement of water solubilization of quercetin by meglumine and application of the solubilization concept to a similar system, J. Mol. Liq. 368 (2022), 120756.
[50] A. Becke, The quantum theory of atoms in molecules: from solid state to DNA and drug design, John Wiley & Sons, 2007.